Pergamon

Available online at www.sciencedirect.com

SCIENCE DIRECT®

Acta Materialia 51 (2003) 3109–3120

Acta MATERIALIA

www.actamat-journals.com

The improvement of high temperature oxidation of Ti–50Al by sputtering Al film and subsequent interdiffusion treatment

M.S. Chu, S.K. Wu *

Department of Materials Science and Engineering, National Taiwan University, 1 Roosevelt Road, Section 4, Taipei 106, Taiwan, ROC

Received 20 August 2002; accepted 27 January 2003

Abstract

The high temperature oxidation resistance of Ti–50Al can be improved by sputtering an Al film and subsequent interdiffusion treatment at 600 °C for 24 h in high vacuum. In these conditions, a $TiAl_3$ layer is formed on the surface, which exhibits good adhesion with Ti–50Al substrate and provides high oxidation resistance. Cyclic and isothermal oxidation tests show that the Ti–50Al with 3–5 μm Al film can dramatically reduce the oxidation at 900 °C in air, at which the parabolic oxidation rate constant K_p of specimen with 5 μm Al film is only about 1/15,000 of that of bare Ti–50Al. XRD and SEM results indicate that the $TiAl_3$ layer can promote the formation of a protective Al_2O_3 scale on the surface as well as react with γ-TiAl to form $TiAl_2$ during the oxidation. Simultaneously, layers of $Al_2O_3/TiAl_2$/Al-enriched γ-TiAl/Ti–50Al are also formed on specimens. The $TiAl_2$ layer thickness will decrease gradually with increasing the oxidation time. After oxidation at 900 °C for 300 h, there is a clearly discontinuous thin layer of $Ti_{37}Al_{53}O_{10}$ compound observed in between Al_2O_3 and $TiAl_2$.

Keywords: Ti–50Al intermetallics; Cyclic oxidation; Sputtering Al thin film; Interdiffusion treatment; $TiAl_3$ and $TiAl_2$ phases

1. Introduction

The γ-TiAl based alloys are one of the most advanced intermetallics, and due to their excellent specific strength at high temperatures, they have successfully demonstrated their potential for aerospace and automotive applications [1–5], such as turbine blades, exhaust valves and turbocharger rotors [5–8]. However, there are still some drawbacks to overcome, such as the limited creep strength and the insufficient oxidation resistance at temperatures above 800 °C. Currently, the maximum target application temperature for this type of material is 900 °C, indicating that efforts must still be performed to improve the high temperature properties [9].

The oxidation of γ-TiAl alloys in air at temperatures above 800 °C does not form a dense Al_2O_3 protective layer on the surface, but rather form a porous TiO_2 layer and a mixture of TiO_2 and Al_2O_3 scales [4,10–12]. Clearly, the excellent oxidation

* Corresponding author. Tel.: +886-2-2363-7846; fax: +886-2-2363-4562.

E-mail address: skw@ccms.ntu.edu.tw (S.K. Wu).

1359-6454/03/$30.00 © 2003 Acta Materialia Inc. Published by Elsevier Science Ltd. All rights reserved.
doi:10.1016/S1359-6454(03)00123-X

resistance of TiAl intermetallics would be due to the formation of a continuous layer, consisting mainly Al_2O_3 in the scale at high temperature. The efforts in the improvement of high temperature oxidation resistance of γ-TiAl include surface modifications and alloying design [13–22]. Many reports indicate that the improvement of oxidation resistance for γ-TiAl favors surface modifications, rather than alloying design [14–20]. It is well-known that the $TiAl_3$ intermetallic shows much better oxidation resistance than γ-TiAl based alloys, because the former has greater aluminum content, resulting in a protective Al_2O_3 layer in the oxidation scale [14,15,23,24]. Therefore, a layer of $TiAl_3$ formed on a γ-TiAl substrate can increase the high temperature oxidation resistance of γ-TiAl. The reported methods for forming a $TiAl_3$ layer on γ-TiAl substrate to resist the high temperature oxidation include aluminum cladding [14], aluminum film deposition by Ion-Beam-Assisted-Deposition [15], and pack cementation aluminizing [16]. However, the improvement of the oxidation resistance is limited due to the poor adhesion of these protective coatings to the substrate, and the intrinsic brittleness of the coatings.

In this study, various thicknesses of pure Al films were first deposited on Ti–50Al alloy by RF magnetron sputtering. Then a subsequent interdiffusion treatment in high vacuum was employed to form a $TiAl_3$ layer on the surface and to increase the adhesion between the thin film and Ti–50Al substrate. Finally, specimens treated by the aforementioned processes were cyclically oxidized at 900 °C in static air and their weight gains were measured. Based on the measured data and the microstructural observations, the improvement of oxidation resistance and the solid-state reaction of $TiAl_3$ and γ-TiAl during high temperature oxidation of Ti–50Al are discussed.

2. Experimental procedures

The Ti–50Al alloy used in this study was prepared as ingots from the raw materials of titanium (99.7%) and aluminum (99.98%) by a vacuum arc remelter (VAR). The ingots were remelted at least six times to promote the homogeneity of the as-cast structure. After homogenization of the ingots at 1000 °C for 100 h, specimens for sputtering were prepared by sectioning the ingots into coupons of dimensions 10 × 10 × 1 mm^3 and 10 × 5 × 1 mm^3. Before sputtering, all surfaces of the specimens were mechanically polished by a standard metallographic procedure to a final polishing of 0.3 μm alumina, then ultrasonically cleaned with acetone and ethanol, and finally rinsed with deionized water. The pure aluminum target for sputtering was also prepared by the same procedure, but the Al ingot was finally sectioned into disk shape of 50 mm in diameter and 5 mm in thickness.

The Al film was deposited on all the surfaces of the Ti–50Al specimens using an RF magnetron sputtering apparatus. The sputtering conditions are given in Table 1, showing that 0.2–5 μm thicknesses of Al films were formed, as measured by α-step (Veeco Dektak^{3}ST). After the sputtering deposition, a subsequent interdiffusion treatment was processed at 600 °C for 24–72 h in a high vacuum of about 3×10^{-7} Torr. Isothermal oxidation tests at 900 °C in static air were performed using a thermogravimetric analysis (TGA, TA Module TGA-DTA 1500). Cyclic oxidation tests were conducted to evaluate the oxidation resistance of γ-TiAl. The specimens were exposed in a muffle furnace at 900 °C for 1–300 h. They were regularly removed from the furnace at time intervals of 5–10 h, air cooled, weighed and returned to the 900 °C furnace. The weight gains per exposed area (mg/cm^2) were measured on an analytical balance to an accuracy of ±0.001 mg (Model: Mettler MT5).

A grazing angle X-ray diffractometer (GAXRD, Siemens D5000) with Cu Kα radiation at 40 kV, 30 mA and 0.03° 2θ/s scanning rate at a grazing angle of 5°, and an X-ray diffractometer (XRD, Philips PW1729) with Cu Kα radiation at 30 kV, 20 mA and 4° 2θ/min scanning rate were used to identify the phases of sputtered films formed by the interdiffusion treatment and by the following oxidation tests. The surface morphologies and cross-sectional microstructures of specimens were observed by a Leo 1530 scanning electron microscopy (SEM) equipped with energy dispersive spectrometry (EDS). An electron probe microanalyzer (EPMA, JEOL JXA-8600 SX) was

Table 1
Sputtering conditions used in this study

System base pressure (Torr)	Sputtering pressure (Torr)	RF power (W)	Sputtering time (min)	Distance between target and substrate (mm)	Al film thickness (μm)
$< 6 \times 10^{-7}$ Torr	5×10^{-3} Torr	100	10–240	80	0.2–5

used for measuring the chemical compositions of phases formed by sputtering, interdiffusion treatment and oxidation tests.

3. Results and discussion

3.1. As-sputtered Al films

Al films with different thicknesses of 0.2–5 μm were sputtered on the Ti–50Al substrate by an RF magnetron sputtering apparatus. Fig. 1(a) and (b) shows the SEM images of top-viewed and cross-sectional morphologies of as-sputtered specimens with a 0.5 μm Al film thickness, respectively. From Fig. 1, the Al film was found to be relatively dense, with extremely small grain size and no visible cracks. In Fig. 1(b), the Al film and the substrate are separated by a crack that occurred when the specimen was cut for SEM cross-sectional observation. This feature indicates that the as-sputtered Al film does not have good adhesion to the substrate. Fig. 2 shows the GAXRD pattern of the as-sputtered Al film, in which only aluminum diffraction peaks are observed. However, the existence of a broad mound at around $2\theta = 20$–$35°$ indicates that as-sputtered Al films are crystalline with a partially amorphous structure.

In order to accurately control the thickness of Al film by sputtering, the sputtering rate of Al film should be determined. According to the sputtering conditions of Table 1 and the thickness measurement of α-step, the sputtering rate of Al film is calculated as approximately 3.5 Å/s. Consequently, the appropriate thickness of Al film can be obtained by controlling the sputtering time, as confirmed by Fig. 3, which shows a linear relationship between sputtering time and film thickness. However, stress inherent in the film increases with increasing the film thickness, resulting in the poor adhesion of coating to substrate. Once the thickness of Al film is over 5 μm, small parts of the film spall out from the Ti–50Al substrate. For this reason, in this study the thicknesses of as-sputtered Al films are all less than 5 μm.

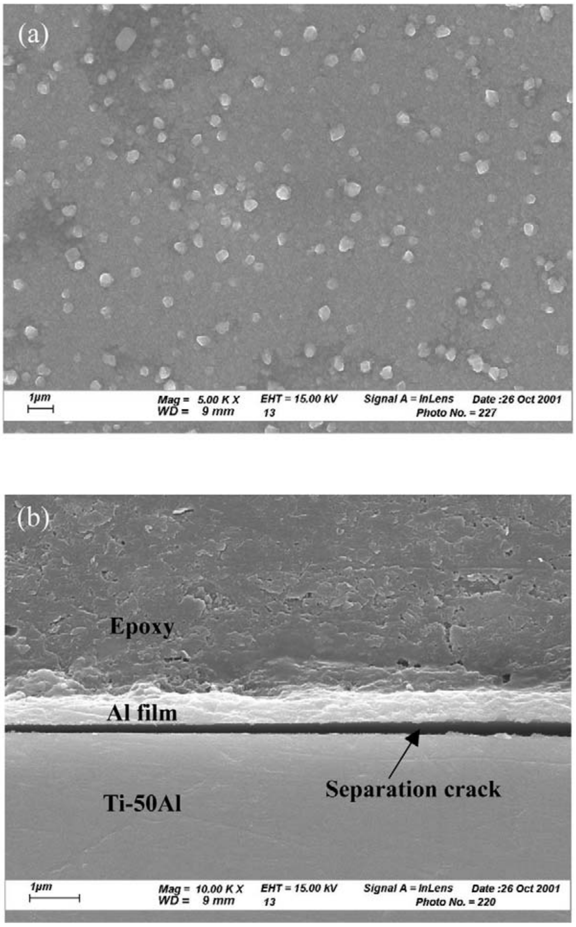

Fig. 1. SEM morphologies of as-sputtered Ti–50Al specimen with 0.5 μm Al film. (a) Surface morphology and (b) cross-sectional morphology.

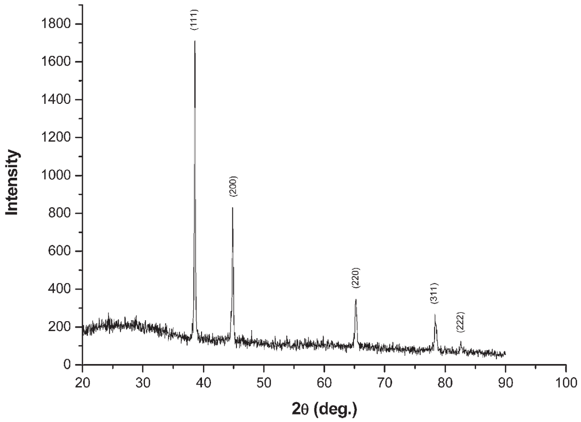

Fig. 2. GAXRD diffraction pattern at 5° grazing angle of incidence of as-sputtered Ti–50Al specimen with 3 μm Al film.

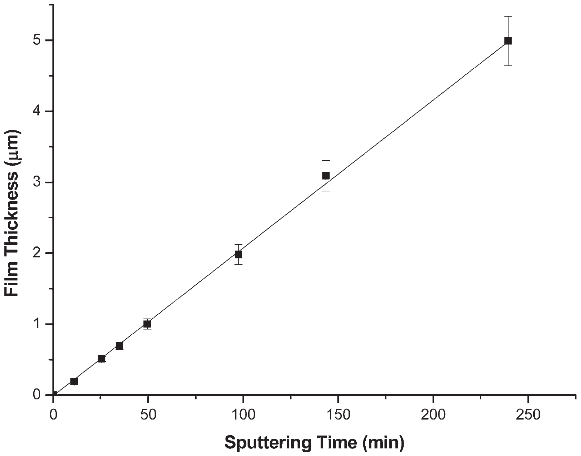

Fig. 3. Plot of the thickness of Al film versus sputtering time.

3.2. Interdiffusion treatment of as-sputtered Al films

In order to form a $TiAl_3$ layer on the Ti–50Al surface and to increase the adhesion between the thin film and Ti–50Al substrate, an interdiffusion treatment is conducted for each specimen sputtered with an Al film. Fig. 4 shows the SEM image of the cross-sectional microstructure of Ti–50Al with a 5 μm thickness of Al film via interdiffusion treatment at 600 °C for 24 h in a vacuum. From Fig. 4, a layer on the outer surface of the substrate can be seen to have a uniform thickness, and no cracks or voids are found at the interface. Thus, this layer

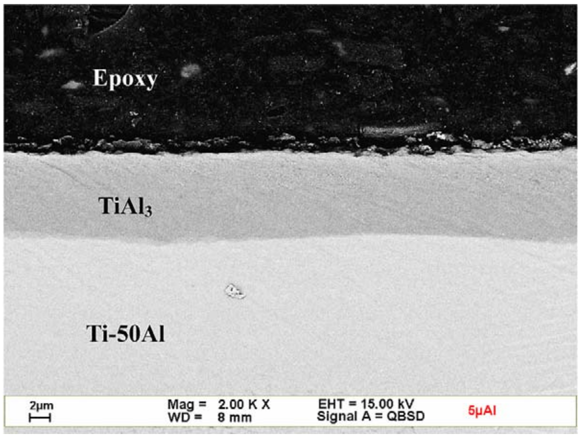

Fig. 4. SEM cross-sectional morphology of Ti–50Al specimen with 5 μm Al film after interdiffusion treatment at 600 °C for 24 h in high vacuum.

exhibits good adhesion with the substrate. From EPMA and EDS tests, this layer has a Al:Ti ratio of 3:1, so it is composed of $TiAl_3$ phase, which is in accordance with the XRD patterns, as shown in Fig. 5. The formation of this $TiAl_3$ layer, according to the diffusion couple test [25] and the Ti–Al phase diagram [26], are due to the following reaction

$$TiAl_{(s)} + Al_{(s)} \rightarrow TiAl_{3(s)} \tag{1}$$

The formation of $TiAl_3$ ceases until all the sputtered Al film is exhausted during the interdiffusion treatment. This means that the thickness of the $TiAl_3$ layer formed by interdiffusion treatment is highly dependent on the thickness of sputtered Al film. It was found that, for a 5 μm thickness of Al film, the thickness of the $TiAl_3$ layer can be extended to about 8 μm by the reaction of Ti–50Al and Al film. From the diffusion couple test of Ti–50Al and Al, the $TiAl_3$ layer can grow rapidly and obey the parabolic time dependence [25]. At the same time, only the thermodynamic stable phase(s) is presented in the end-product [27–29]. This feature shows why this $TiAl_3$ layer will further react with γ-TiAl to form $TiAl_2$ after 900 °C oxidation, as discussed in Section 3.4.

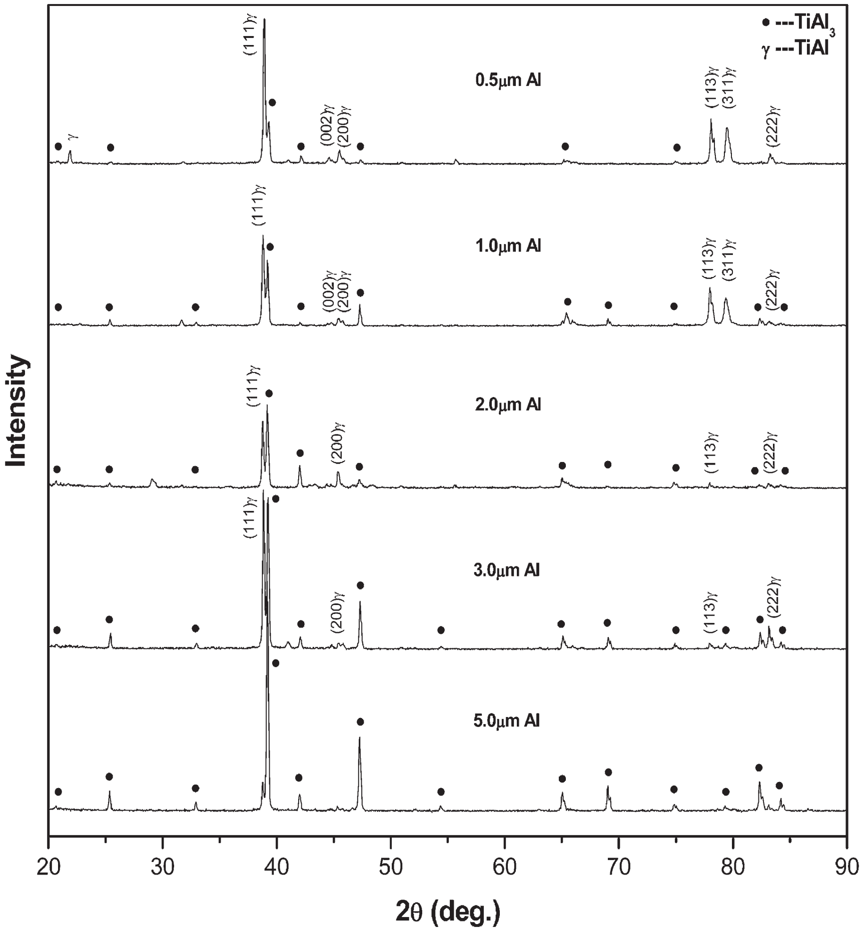

Fig. 5. The XRD diffraction spectra of Ti–50Al specimens with various thicknesses of Al films (from 0.5 to 5 μm) after interdiffusion treatment at 600 °C for 24 h in high vacuum.

3.3. Cyclic and isothermal oxidation

The cyclic oxidation tests were carried out at 900 °C in static air for 80 h. Each cycle consisted of heating up to 900 °C, holding at 900 °C for 5 or 10 h and then cooling to room temperature. Only the time period of the specimen exposed at 900 °C is counted in the cyclic oxidation test. The oxidation weights were measured from the weight change of the tested specimens, including the remaining and exfoliated scales. Fig. 6 shows the (weight change per unit area)^2 versus the oxidation time at 900 °C air for Ti–50Al specimens with and without Al film. All specimens with sputtered Al film had processed the interdiffusion treatment at 600 °C for 24 h in a vacuum. Fig. 6 indicates that the thickness of Al film is a major factor in the improvement of oxidation resistance of γ-TiAl. Clearly, Ti–50Al specimens with 3 and 5 μm Al films have excellent oxidation resistance at 900 °C. This comes from the fact that they have a sufficient thickness of $TiAl_3$ layer, which can form an adhesive and continuous Al_2O_3 scale on the outer surface during cyclic oxidation. At the same time, no scale spalling occurs during the cyclic oxidation for specimens with 3 and 5 μm Al films. On the other hand, the specimens with thinner Al film, especially with thickness <1 μm (including the bare Ti–50Al) have the scale spalling during the oxidation. This results from the formation of outer

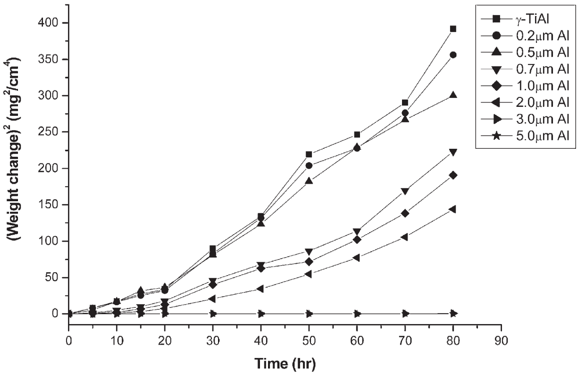

Fig. 6. Cyclic oxidation tests in static air at 900 °C for Ti–50Al specimens with various thicknesses of Al films which have been interdiffusion treated at 600 °C for 24 h in high vacuum.

TiO_2 layer, and the degree of spalling decreases with increasing the thickness of Al film. The parabolic oxidation rate constant, K_p, can be calculated from the curve fitting of Fig. 6, and this constant is used as a convenient index for comparing the improvement of oxidation resistance.

Fig. 7 shows the calculated K_p values versus Al film thickness. The K_p value for the cyclic oxidation of 3 μm Al film at 900 °C is 0.00709 mg^2/(cm^4 h), in contrast to 4.899 mg^2/(cm^4 h) for the bare Ti–50Al. The K_p value for the former one is about 1/700 of the latter one. Furthermore, the K_p value for the cyclic oxidation of 5 μm Al film at 900 °C can be further reduced to 3.2×10^{-4} mg^2/(cm^4 h), which is about 1/15,000 of K_p value for the bare Ti–50Al. In other words, oxidation resistance of Ti–50Al with 5 μm Al film can be improved dramatically by about four orders of magnitude, as compared to Ti–50Al without Al film. The results of Fig. 7 indicate that the increase in Al film thickness leads to the decrease in K_p value, that is, it enhances the oxidation resistance of Ti–50Al. However, the improvement of oxidation resistance is limited when the Al film thickness is less than 2 μm. This may be because the thickness of $TiAl_3$ layer is not thick enough to protect against the diffusion of oxygen into the substrate.

Isothermal oxidation tests were performed by TGA at 900 °C for 70 h to compare oxidation properties of Ti–50Al with and without Al film, as shown in Fig. 8. From Fig. 8, the sputtered Al film and subsequent interdiffusion treatment can substantially reduce the oxidation rate of Ti–50Al. This result is in accordance with the cyclic oxidation results of Fig. 6. The K_p value calculated from the curves of Fig. 6 and Fig. 8 under the same Al film thickness is nearly equivalent. Also note that from Fig. 8, the oxidation curve of bare Ti–50Al does not completely obey the parabolic law for all oxidation times. However, in the case of Ti–50Al with Al film, the oxidation behavior seems to be quasi-linear in the early oxidation time, and

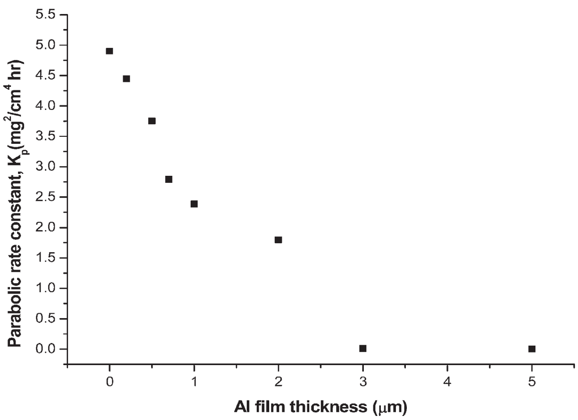

Fig. 7. Effect of the thickness of Al film on the cyclic oxidation resistance (parabolic rate constant K_p) of Ti–50Al specimens oxidized in 900 °C air. The K_p values are calculated from Fig. 6.

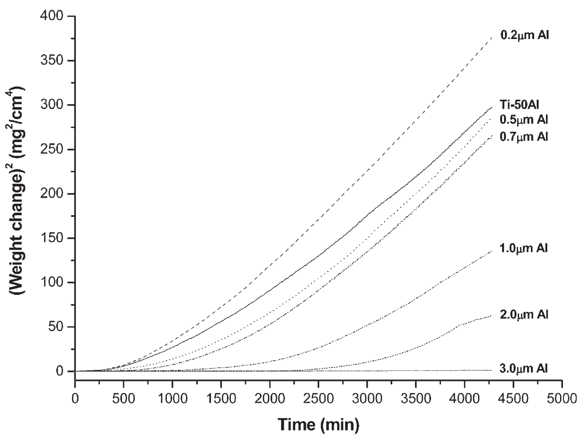

Fig. 8. TGA isothermal oxidation tests in static 900 °C air for Ti–50Al specimens with various thicknesses of Al films.

then gradually shifts toward the parabolic law. This behavior is especially significant in specimen with 3 μm Al film, so that the mass gain of this specimen is reduced dramatically.

3.4. Cross-sectional microstructure observations of specimens after cyclic oxidation

To identify the phases developed after cyclic oxidation test in Ti–50Al specimens with outer $TiAl_3$ layer, the specimens were analyzed by XRD. Fig. 9 shows the XRD spectra of Ti–50Al specimens with Al film which have been interdiffusion treated at 600 °C for 24 h and cyclically oxidized at 900 °C in air. The XRD pattern of the bare Ti–50Al specimen is also shown in Fig. 9, in which except for the γ-TiAl peaks, only TiO_2 (rutile) peaks are found. For specimens with a 1 μm Al film, the peaks for Al_2O_3, TiO_2 and $TiAl_2$ phases are identified. This indicates that the formed oxides consist of a mixture of Al_2O_3 and TiO_2. Moreover, the appearance of $TiAl_2$ peaks indicates that $TiAl_3$ has reacted with γ-TiAl to form $TiAl_2$ at 900 °C oxidation. When the thickness of Al film increases, i.e. the $TiAl_3$ layer becomes thick, the peak intensities for Al_2O_3 and $TiAl_2$ become strong, whereas those for TiO_2 become weak. For the Ti–50Al specimen with 5 μm Al film, the XRD spectrum shows only Al_2O_3 and $TiAl_2$ peaks, implying that a protective alumina scale, instead of a fragile TiO_2

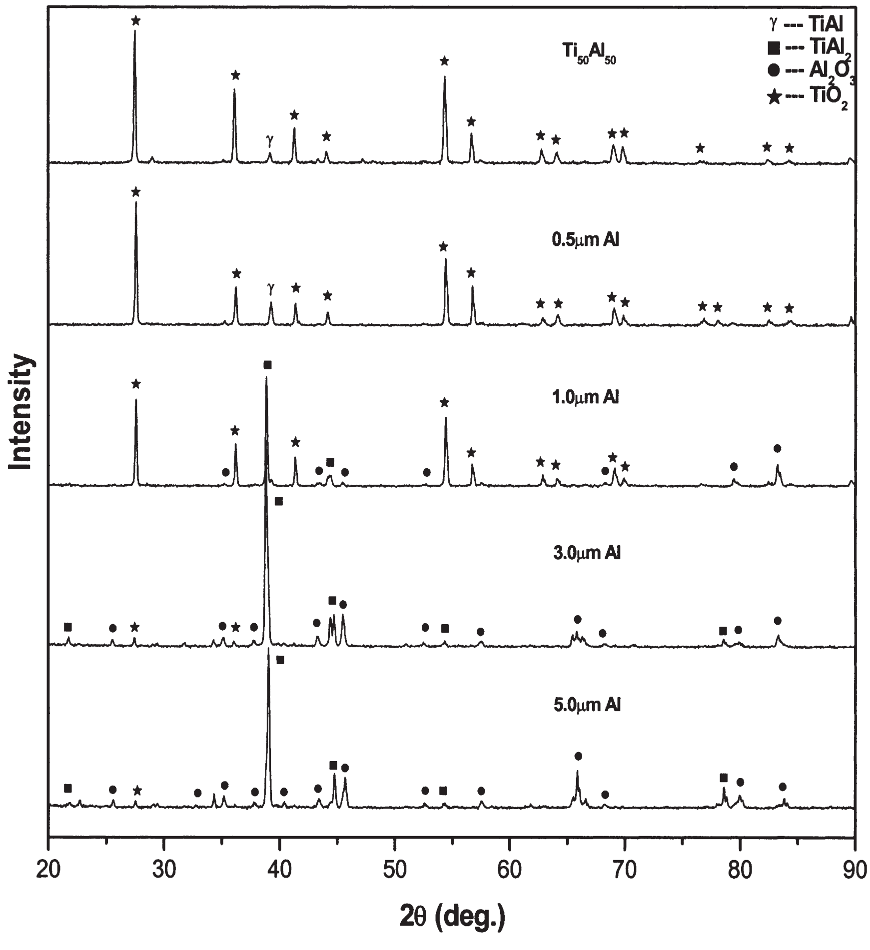

Fig. 9. XRD diffraction spectra of Al-sputtered Ti–50Al specimens after interdiffusion treatment and then oxidation at 900 °C for 80 h in air. The thickness of Al film ranges from 0 (bare Ti–50Al) to 5 μm.

one, is formed on the outer surface of the specimen. At the same time, $TiAl_2$ reacted from $TiAl_3$ beneath the alumina scale is formed, as discussed further below. Fig. 9 indicates that the improvement of oxidation resistance of Ti–50Al is mainly dependent on the $TiAl_3$ thickness. The thicker the $TiAl_3$ layer is, the more high temperature oxidation resistance is obtained. From Figs 6–9, the minimum thickness of the $TiAl_3$ layer is about 5 μm, i.e. that of the sputtered Al film is about 3 μm, to obtain the sufficient high temperature oxidation resistance for Ti–50Al alloy.

Fig. 10(a) and (b) shows the top-viewed SEM morphologies of Ti–50Al-sputtered 0.5 and 3 μm Al films, respectively, which have been interdiffusion treated at 600 °C for 24 h in a vacuum, and then cyclically oxidized at 900 °C for 80 h in air. Fig. 10(a) reveals that, for the 0.5 μm Al film specimen, only large quantities of TiO_2 crystal formed on the surface. The thinness of the Al film causes the $TiAl_3$ to be not thick enough to form a stable Al_2O_3 layer in the scale. In contrast, on the 3 μm Al film specimen of Fig. 10(b), a stable Al_2O_3 layer has formed on the outmost part of the oxide scale, as shown in Fig. 9. This Al_2O_3 layer becomes a good barrier against inward and outward diffusion, resulting in improved oxidation resistance of Ti–50Al at 900 °C in air.

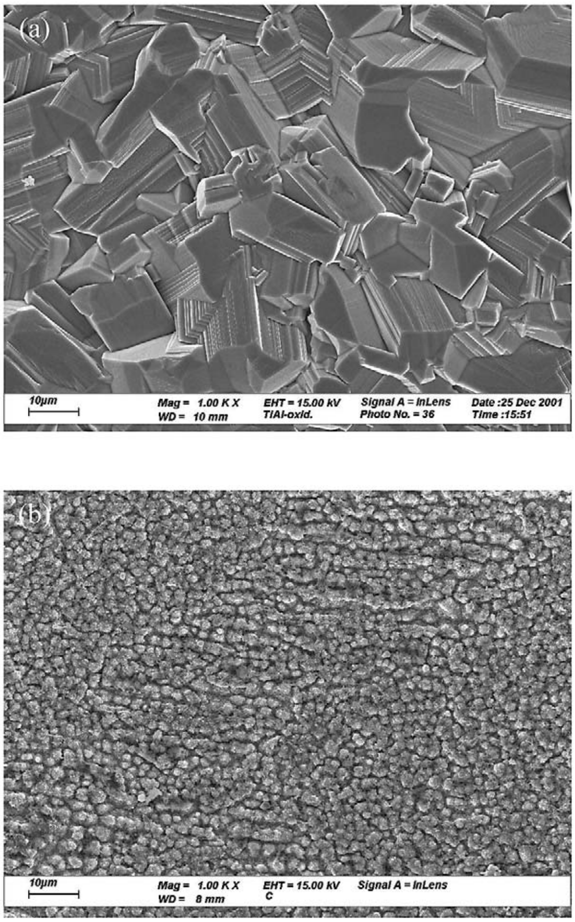

Fig. 10. SEM surface morphologies of the oxidation scale after 900 °C × 80 h oxidation for (a) 0.5 μm Al film and (b) 3 μm Al film. The specimens were interdiffusion treated in high vacuum before the oxidation.

The cross-sectional microstructures of the same specimens of Fig. 10(a) and (b) were observed by SEM, as shown in Fig. 11(a) and (b), respectively. Fig. 11(a) reveals that the microstructure is almost the same as the bare Ti–50Al specimen, i.e. a very thick oxide scale is formed with an outmost rutile layer and several different layers beneath it, such as a mixture of TiO_2 and Al_2O_3 oxides [30]. From Fig. 11(b), the microstructure of the specimen with a 3 μm Al film is uncomplicated. Three layers coexist in Fig. 11(b), as shown by the accompanying EDS analysis. The outer layer is Al_2O_3, the middle one is $TiAl_2$ (point 1 of Fig. 11(b)) and the inner layer is Al-enriched γ-TiAl (points 2, 3 and 4 of Fig. 11(b)). An adhered Al_2O_3 scale forms on the surface of $TiAl_2$ layer and provides excellent protection against oxidation attack. As to the $TiAl_2$ formation, it appears to be reacted from $TiAl_3$ and γ-TiAl [29], as confirmed by XRD spectra shown in Fig. 9. The Al-enriched γ-TiAl phase is just the same structure as γ-TiAl but its Al content is higher than 50 at.% [26]. In Al-enriched γ-TiAl layer, the closer the position to $TiAl_2$ layer, the more Al content it has, as quantitatively shown in Fig. 11(b) by EDS analysis. The stability of the $TiAl_2$ phase will be further discussed in Section 3.5.

3.5. *$TiAl_2$ phase versus oxidation time*

It has been reported that, in the study of diffusion couples, the $TiAl_2$ phase can be formed by reaction at the interface between γ-TiAl and $TiAl_3$ alloys at high temperature [25]. In this study, $TiAl_3$

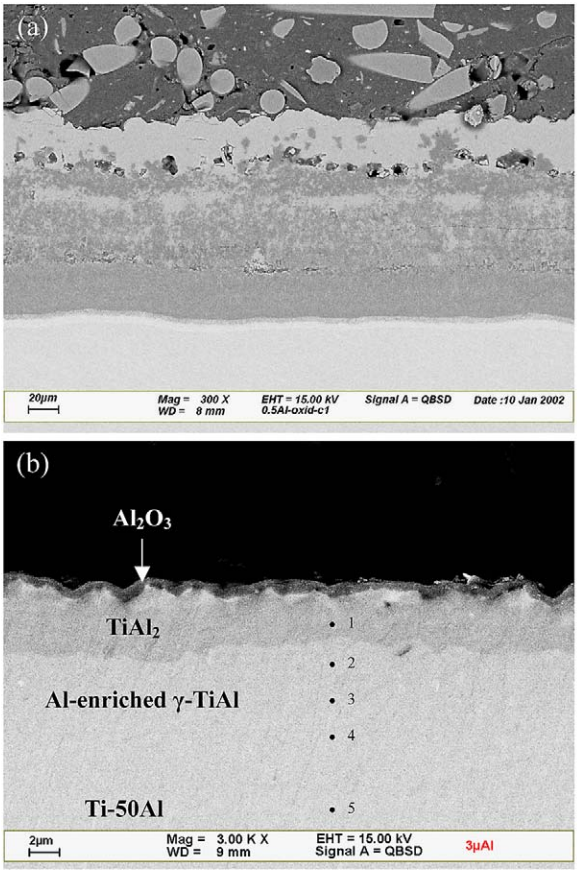

	Composition			
Location	Ti (at. %)	Al (at. %)	O (at. %)	phase
Point 1	33.44	66.56	--	$TiAl_2$
Point 2	42.15	57.85	--	Al-enriched γ-TiAl
Point 3	43.64	56.36	--	Al-enriched γ-TiAl
Point 4	45.68	54.32	--	Al-enriched γ-TiAl
Point 5	50.25	49.75	--	Ti-50Al

Fig. 11. SEM cross-sectional images of the specimens of Fig. 10 for (a) 0.5 and (b) 3 μm Al film. The accompanying EDS analysis for the composition of points 1–5 shown in (b) is also listed.

can totally react with γ-TiAl to form $TiAl_2$ phase after oxidation at 900 °C for 80 h in air, as demonstrated in Section 3.4. However, with increasing oxidation time, the thickness of the $TiAl_2$ layer decreases due to the solid-state diffusion with Ti–50Al at high temperature. In order to realize the stability of the $TiAl_2$ phase, Ti–50Al specimens with 5 μm Al film via interdiffusion treatment and then oxidation at 900 °C for various times were investigated and their cross-sectional SEM images are shown in Fig. 12. From Fig. 12(a), it can be seen that in the initial period of oxidation time (1 h at 900 °C), a mixture of $TiAl_3$ outer layer and $TiAl_2$ inner layer coexists. This indicates that $TiAl_2$ is reacted from $TiAl_3$ and γ-TiAl, as we proposed in Section 3.4. Comparing the thickness of the $TiAl_2$ layer to that of $TiAl_3$ layer, as shown in Fig. 12(a), one can find that the reaction rate between $TiAl_3$ and γ-TiAl is rapid and it is completed within 2 h. This result is similar to the case of the diffusion couple [25] in which the $TiAl_2$ formation requires about 4 h at 750 °C.

In Fig. 12, Al_2O_3 scale formed on the Ti–50Al is not completed in the initial oxidation period, but it reveals that a continuous Al_2O_3 scale can be formed with further oxidation time. Meanwhile, the thickness of the $TiAl_2$ layer decreases as the oxidation time increases. After 300 h oxidation, as shown in Fig. 12(f), the thickness of the $TiAl_2$ layer is reduced to only about 5.5 μm in thickness. Because the $TiAl_2$ can be exhausted eventually, and from the thickness measurement of the $TiAl_2$ layer of Fig. 12(b)–(f), one can estimate that the exhaustion time of the $TiAl_2$ layer at 900 °C for a specimen with a 5 μm Al film is about 700 h.

Table 2 lists the cross-sectional EDS analysis of the specimen of Fig. 12(f) which has been oxidized at 900 °C for 300 h. These results are quite similar to those of Fig. 11(b) except that now there is a clearly discontinuous thin layer in between Al_2O_3 and $TiAl_2$, as shown by points 1 and 2 of Fig. 12(f). The EDS results of points 1 and 2 indicate that this layer is a Ti–Al–O compound with its composition approximating $Ti_{37}Al_{53}O_{10}$. Since this compound has not been reported yet, further study is needed to identify its exact composition and structure.

4. Conclusions

The high temperature oxidation resistance of Ti–50Al can be improved by a sputtered Al film and subsequent interdiffusion treatment at 600 °C for 24 h in high vacuum. The as-sputtered Al films can have their thicknesses controlled accurately by magnetron sputtering process, and they reveal a crystalline with partially amorphous structure.

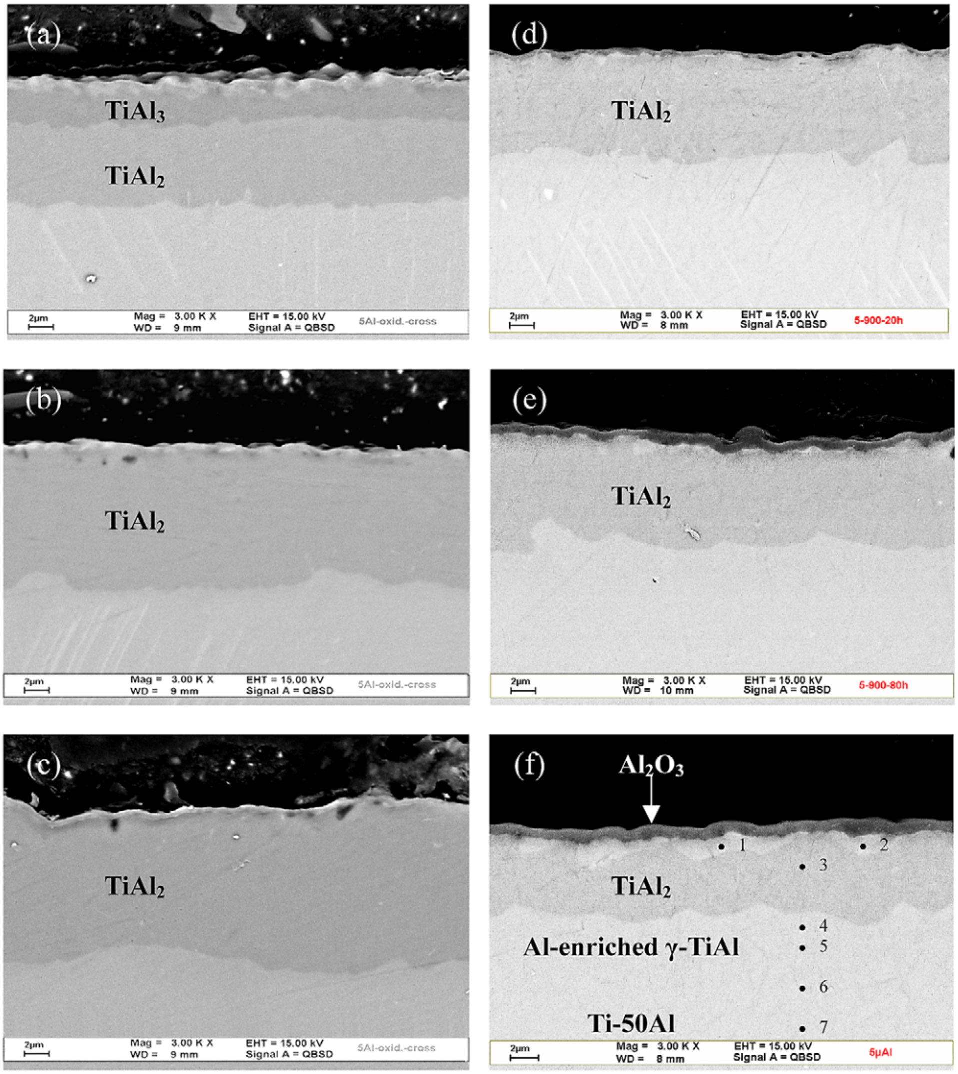

Fig. 12. SEM cross-sectional images of Ti–50Al specimens with 5 μm Al films which have been interdiffusion treated, and then oxidized at 900 °C in air for (a) 1 h (b) 5 h (c) 10 h (d) 20 h (e) 80 h and (f) 300 h. The EDS analysis for the composition of points 1–7 shown in (f) is listed in Table 2.

However, when the Al film thickness exceeds 5 μm, small parts of film can be spalled out from the substrate, hence its thickness is limited to less than 5 μm in this study. A $TiAl_3$ layer is formed on the surface of the Ti–50Al substrate after interdiffusion treatment of the Al-sputtered specimens. This $TiAl_3$ layer exhibits good adhesion with the substrate and plays an important role in the long-term oxidation resistance. Cyclic and isothermal oxidation tests at 900 °C in air indicate that the Ti–50Al with $TiAl_3$ layer can dramatically reduce the oxidation rate if the sputtering thickness of Al film can reach 3–5 μm. The parabolic rate constant K_p of specimens with 3 and 5 μm Al film thickness can be reduced to about 1/700 and 1/15,000, respectively, as compared to that of bare Ti–50Al. From the results of XRD and SEM + EDS of cyclic oxidized specimens, it can be seen that the $TiAl_3$ layer not only promotes the formation of a continuous Al_2O_3 scale on the outer surface, but it also

Table 2
EDS analysis of Fig. 12(f) for the composition of points 1–7

Location	Composition			
	Ti (at. %)	Al (at. %)	O (at. %)	Phase
Point 1	36.03	52.85	11.11	Ti–Al–O compound
Point 2	36.46	53.51	10.03	Ti–Al–O compound
Point 3	33.66	66.34	–	$TiAl_2$
Point 4	41.14	58.86	–	Al-enriched γ-TiAl
Point 5	43.55	56.45	–	Al-enriched γ-TiAl
Point 6	45.56	54.44	–	Al-enriched γ-TiAl
Point 7	49.75	50.25	–	Ti–50Al

reacts with γ-TiAl to form $TiAl_2$ during the oxidation. $TiAl_2$ then reacts with Ti–50Al to form an Al-enriched γ-TiAl layer. The reaction rate of $TiAl_3$ with γ-TiAl to form $TiAl_2$ is rapid and will be completed within 2 h. Experimental results show that the thickness of $TiAl_2$ layer decreases gradually with increasing oxidation time, indicating that it will be eventually exhausted. For specimens with 3–5 μm Al film, after the $TiAl_2$ has formed, the cross-sectional observations show that there are layers of Al_2O_3/$TiAl_2$/Al-enriched γ-TiAl/Ti–50Al. If the oxidation time reaches 300 h, in addition to the aforementioned layers, there is a discontinuous thin layer of $Ti_{37}Al_{53}O_{10}$ compound formed in between the Al_2O_3 and $TiAl_2$.

Acknowledgements

The authors gratefully acknowledge the financial support for this research provided by the National Science Council (NSC), Taiwan, Republic of China, under Grant Nos. NSC89-2218-E002-071 and NSC90-CS-7-082-001.

References

[1] Zhang WJ, Reddy BV, Deevi SC. Scripta Mater 2001;45:645.
[2] Yamaguchi M, Inui H, Ito K. Acta mater 2000;48:307.
[3] Liu CT. In: Baker I, Darolia R, Whittenberger JD, Yoo M, editors. High-temperature ordered intermetallic alloys V. Pittsburgh, PA: MRS. 1993. p. 3.
[4] Kim YW. JOM 1994;41:30.
[5] Tetsui T, Ono S. Intermetallics 1997;7:689.
[6] Noda T. Intermetallics 1998;6:709.
[7] Eylon D, Keller MM, Jones PE. Intermetallics 1998;6:703.
[8] Clemens H, Kestler H. Adv Eng Mater 2000;2:551.
[9] Kim YW, Dimiduk DM. In: Nathal MV, Darolia R, Liu CT, Martin PL, Miracle DB, Wagner R, Yamaguchi M, editors. Structural intermetallics. Warrendale, PA: TMS; 1997. p. 531.
[10] Yang MR, Wu SK. J Oxid Metals 2000;54:473.
[11] Becker S, Rahmel A, Schorr M, Schutze M. Oxid Metals 1992;38:425.
[12] Dimiduk DM, Miracle DB, Ward CH. Mater Sci Technol 1992;8:367.
[13] Yang MR, Wu SK. Acta Mater 2002;50:691.
[14] Hsu IC, Wu SK, Lin RY. Mater Chem Phys 1997;49:184.
[15] Li XY, Zhu YC, Fujita K, Iwamoto N, Matsunaga Y, Nakagawa K et al. Surf Coat Technol 2001;136:276.
[16] Yoshida Y, Anada H. High temperature corrosion of advanced materials and protective coating. New York: Elsevier, 1992.
[17] Kim JP, Jung HG, Kim KY. Surf Coat Technol 1999;112:91.
[18] Tang Z, Niewolak L, Schemet V, Singheiser L, Quadarkker WJ, Wang F et al. Mater Sci Eng A 2002;328:297.
[19] Lee JK, Oh MH, Wee DM. Intermetallics 2002;10:347.
[20] Zhou C, Yang Y, Gong S, Xu H. Mater Sci Eng A 2001;307:182.
[21] Skowronski RP. J Am Ceram Soc 1994;77:1098.
[22] Schumacher G, Dettenwanger F, Schutzem, Hornauer U, Richter E, Wieser E et al. Intermetallics 1999;7:1113.
[23] Yoshihara M, Tanaka R. Materia Japan 1991;30:61.

[24] Welsch G, Khevci AI. In: Grobstein T, Doychak J, editors. Oxidation of high temperature inter-metallics. Warrendale, PA: TMS; 1989. p. 207.
[25] van Loo FJJ, Rieck GD. Acta Metall 1973;21:73.
[26] ASM handbook, vol. 3. Alloy phase diagrams. Metal Park, OH: ASM International; 1992.
[27] Palm M, Zhang LC, Stein F, Sauthoff G. Intermetallics 2002;10:523.
[28] Kattner UR, Lin JC, Chang YA. Metall Trans A 1992;23:2081.
[29] Pretorius R, Marais TK, Theron CC. Mater Sci Eng 1993;10R:1.
[30] Schmitz-Niederau M, Schutze M. Oxid Metals 1999;52:225.